Cement and Concrete Research 42 (2012) 700–709

Contents lists available at SciVerse ScienceDirect

Cement and Concrete Research

journal homepage: http://ees.elsevier.com/CEMCON/default.asp

Shear transfer across a crack in recycled aggregate concrete

Jianzhuang Xiao [a,*], He Xie [a], Zhenjun Yang [b]

[a] Department of Building Engineering, Tongji University, Shanghai, 200092, PR China
[b] School of Mechanical, Aerospace and Civil Engineering, the University of Manchester, Manchester, M13 9PL, UK

ARTICLE INFO

Article history:
Received 29 July 2011
Accepted 15 February 2012

Keywords:
Concrete (E)
Aggregate (D)
Mixture proportioning (A)
Crack (B)
Shear transfer strength across cracks

ABSTRACT

In this paper, 32 pre-cracked recycled aggregate concrete (RAC) push-off specimens made from 10 mix designs were tested to study the shear transfer performance across cracks. The effects of recycled coarse aggregate (RCA) replacement ratio, the water to cement ratio, the concrete strength, and the lateral constraint on the shear transfer performance were carefully investigated. The experimental results and data analysis show that the shear transfer mechanism and process across cracks in RAC is largely the same as that in natural aggregate concrete (NAC). Both the lateral constraint and the concrete compressive strength positively affect the shear transfer strength of the RAC. However, the RCA replacement ratio has adverse effects on the shear transfer strength when it is over 30%. It is also found that the design equations for NAC in ACI and PCI codes may be used to predict the shear transfer strength of RAC.

1. Introduction

To combat global warming by reducing carbon footprint, recycled aggregate concrete (RAC) has received much attention recently in the construction research community. In RAC, coarse aggregates recycled from demolished concrete structures are embedded in virgin cement mortar. Because the recycled coarse aggregates (RCAs) are usually wrapped by a layer of old, weak mortar that cannot be completely removed during the recycling process, an updated mix proportion design method is often used to compensate the weaker bonding between the RCAs and mortar so that comparable material strength can be achieved. However, a better understanding of the mechanical properties and failure mechanisms of RAC under different loading conditions is still urgently needed before it can be confidently used in practical design. One hardly investigated aspect is the RAC's shear transfer capability across cracks, which is the focus of this study.

It is well known that the shear transfer capability across cracks in concrete, through mechanisms such as crack surface friction, aggregate interlock and dowel action, contributes significantly to the shear strength of structures such as deep reinforced concrete beams, corbels, and shear walls [1]. It has been taken into account in major design codes such as Eurocode 2 by empirical equations after decades of experimental and analytical research. It is well known that cracks generally develop along interfaces between coarse aggregates and mortar. When a crack is subjected to shear deformation, the projecting coarse aggregates on one side of the crack will become in contact with the mortar on the other side, resulting in compression and friction between the aggregates and the mortar, namely, the aggregate interlock across the crack [2]. When the crack width is small, shear stress across the crack can be transferred by the aggregate interlock; as the crack opens gradually, the aggregate interlock effect diminishes. This is the mechanism of aggregate interlock in concrete.

Both shear tests on concrete members and interface shear tests designed to study shear transfer [3–7] confirm that the shear force across cracks in concrete is mainly transferred by aggregate interlock. From the macro perspective, the aggregate interlock is mainly affected by the crack width, the concrete strength and lateral constraint stiffness; from the micro perspective, it is transferred by local contact surfaces between the coarse aggregates on one side of cracks and the mortar on the other side. Therefore, the volume density of the coarse aggregates and the mechanical properties of the mortar are predominant factors in the aggregate interlock and the shear transfer capabilities across cracks in concrete. In the RAC, more coarse aggregates in unit volume are used and the mortar surrounding the RCAs is weaker than that in normal concrete. These may have profound implications on the aggregate interlock and shear transfer capabilities across cracks. However, no shear transfer tests on RAC have been carried out so far.

A few physical models have been proposed to account for the aggregate interlock in concrete. Laible et al. [8] considers two stages in the aggregate interlock mechanism. At the initial stage of crack propagation, the aggregate interlock force is caused by the “local rough” contact between the mortar surrounding the aggregates on one side of the crack and the mortar on the other side. At the late stage of crack propagation, the mortar wrapping the aggregate is crushed and the aggregate interlock comes from the “global rough” contact between the aggregates and the mortar. The models proposed in

* Corresponding author. Tel: +86 21 65982787; fax: +86 21 65986345.
E-mail address: jzx@tongji.edu.cn (J. Xiao).

0008-8846/$ – see front matter © 2012 Elsevier Ltd. All rights reserved.
doi:10.1016/j.cemconres.2012.02.006

Table 1
Grading of recycled coarse aggregates: mesh analysis and calculation.

(Sample mass = 6300 g).

Mesh size (mm)	Retained amount (g)	Accumulate retained amount (g)	Accumulate retained rate (%)
31.5	0	0	0
26.5	26	26	0.4
19	955	981	15.6
16	809	1790	28.4
9.5	2248	4038	64.1
4.75	1905	5943	94.3
2.36	278	6221	98.7
<2.36	76	6297	100

Refs. [9] and [10] stipulate that the aggregate interlock across cracks is entirely due to the sliding friction between two rigid bodies with contacting surfaces approximated by combs or a series of parabolic curves. Walraven and Reinhardt [3] proposed a more sophisticated model by treating concrete as a two-phase material consisting of coarse aggregates and the cement mortar. The aggregates are modeled as rigid spheres of different size embedded in the plastic deformable mortar on both sides of cracks at different depths. When the shear deformation and crack propagation occur, the friction force at the crack surface and the pressing force can be obtained by solving the force equilibrium equations. If the lateral constraint stiffness is known, the crack width and the development of shear displacement-shear load relationship can also be calculated. They also obtained the most probable distribution of the local contact surface between the projecting coarse aggregates across a crack and the mortar on the other side, and the random distribution of the projecting coarse aggregates' embedded depths, through probability analysis. In recent years, some investigators have undertaken some numerical simulation on aggregate interlocking of concrete instead of lab experiments [11]. Haskett et al. [12] proposed new equations to consider aggregate interlock behaviour across sliding planes in cracked and uncracked concrete. Generally speaking, in the numerical modeling, the aggregate interlock is very difficult to be modeled explicitly.

2. Research significance

As recycled coarse aggregates have old mortar attached to their surfaces and more aggregates in unit volume are used in RAC, the mechanism of aggregate interlock across cracks and the shear stress transfer capability in RAC are expected to be different from those in natural aggregate concrete (NAC). Furthermore, micro-cracks and internal damage already exist in recycled concrete materials before they are mixed with new mortar. They may have adverse impact on RAC's aggregate interlock capability. The effects of the above factors in RAC have not yet been investigated, which severely limits its wide use. This study aims to elucidate the effects of key factors on the aggregate interlock capability of RAC by carefully designed laboratory tests of 32 pre-cracked pull-off specimens with different parameters such as aggregate types, concrete strength, lateral constraint stiffness etc.

Table 2
Basic property of coarse aggregates.

Aggregate	Crush index (%)	Volume density (kg m^{-3})	Apparent density (kg m^{-3})	Water absorption (%)	Soil content (%)
RCA	10.0	1320	2500	5.6	3.5
NCA	3.5	1465	2810	0.6	0.9

Table 3
Mechanical properties of steel.

Steel bar	Φ8 (HPB235)	Φ14(HRB335)
Yield strength f_y (MPa)	340.0	549.4
Modulus of elasticity E (GPa)	210.9	196.0

3. Experimental design

3.1. Material

Both recycled coarse aggregates (RCAs) and natural coarse aggregates (NCAs) were used in the tests. The gradation of RCAs is listed in Table 1. The NCAs are crushed stones with continuous grading. The basic properties of both types of aggregates are shown in Table 2. The PO42.5 Portland cement was used with tap water and JC-3 water-reducing admixture. The sand used was general velvet. The steel bars used were HPB235 (only for stirrups) and HRB335 hot-rolled steel with mechanical properties determined by uniaxial tensile tests and listed in Table 3.

10 mix types with various RCA replacement ratio (R_r) and water to cement ratios were designed in the test, as listed in Table 4. The first 3 have the same water to cement ratio and different R_r, the next 2 have no RCAs, the next 2 have no NCAs, and the rest 3 have a mixture of both aggregates with varying R_r.

3.2. Specimen design

32 shear push-off specimens of the same size, shown in Fig. 1, were designed and cast. To ensure that the crack initiates and propagates in the shear plane (the shaded area in Fig. 1), two 300mm long, 15mm deep v-slots were made when the concrete was cast, resulting in a shear plane area $A_c = 36{,}000$ mm^2.

Horizontal bars across the crack in the form of closed stirrups were used to simulate the lateral constraint, as shown in Fig. 2. Two to four stirrups were used in different specimens to model different lateral constraint stiffness. To reduce the contribution of the stirrups' dowel action to the shear strength, the stirrups were wrapped with soft tubes of 40 mm length.

The basic information of the 32 specimens is listed in Table 5. Each specimen is given a unique name with a letter and digits. The letter and the digits before the hyphen sign identify the source of aggregates, with R for RCAs, N for NCAs, and the digits following R for RCA's replacement ratio R_r (R without digits followed means 100% replacement ratio in mass). The first digit after the hyphen sign indicates the mix type in

Table 4
Mixture proportions of recycled aggregate concrete.

No.	RCA replacement ratio (%)	Cement (kg)	Sand (kg)	NCA (kg)	RCA (kg)	Water (kg)	Water–cement ratio
Mix 1a	0	373	730	1120	0	182	0.488
Mix 1b	50	373	730	560	560	182	0.488
Mix 1c	100	373	730	0	1120	182	0.488
Mix 2	0	370	730	1100	0	200	0.540
Mix 3	0	440	720	1050	0	190	0.430
Mix 4	100	430	700	0	950	185	0.430
Mix 5	100	430	700	0	1000	165	0.380
Mix 6	30	400	710	742	318	185	0.463
Mix 7	50	406	730	510	510	185	0.456
Mix 8	70	415	720	300	700	185	0.446

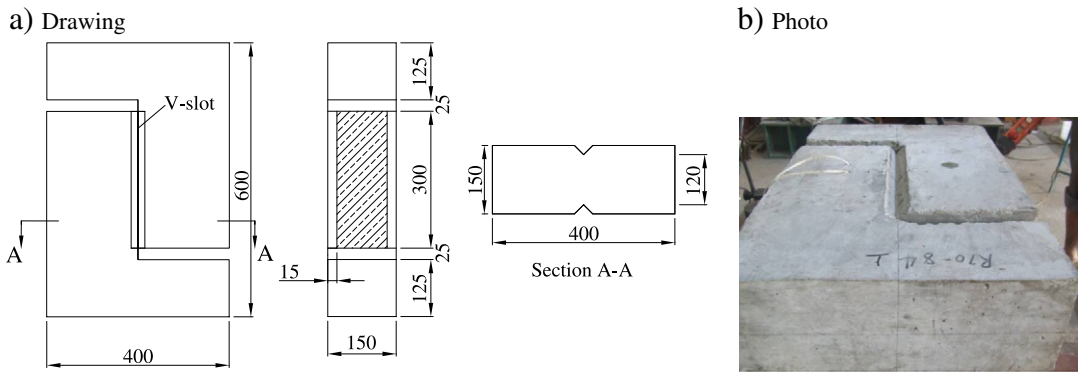

Fig. 1. Geometry and dimensions of the shear push-off specimens.

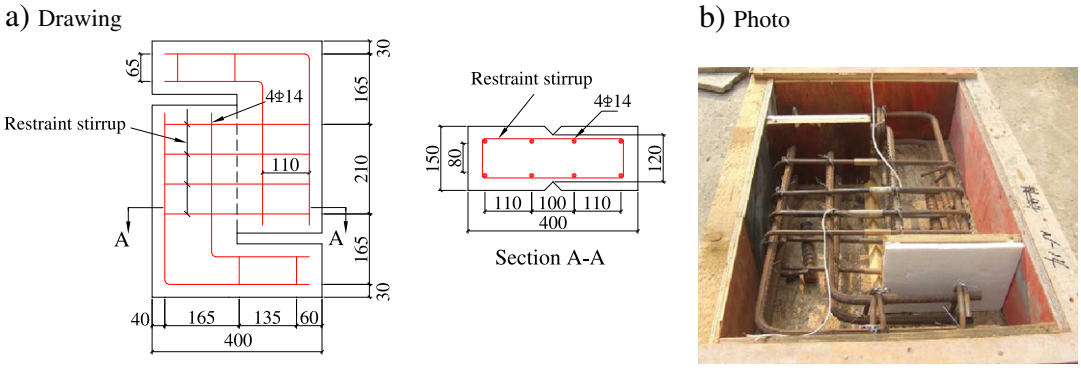

Fig. 2. Reinforcement in the specimens.

Table 4, and the second digit indicates the number of stirrups passing through the shear plane.

3.3. Fabrication and curing of specimens

The formwork was placed horizontally and the concrete was cast along the specimen thickness direction. Two 300 mm long battens with an equilateral triangle cross-section were used to make the v-slots. A finished specimen after 28-day curing at room temperature is shown in Fig. 1b.

3.4. Testing facility

All the tests were carried on in the Laboratory of Building Structures at Tongji University, Shanghai, China. Before the push-off shear tests were conducted, all the specimens were pre-cracked using the test rig shown in Fig. 3a. The specimen was carefully placed horizontally. The vertical loading was applied gradually until a cleavage crack appeared or the strain in the stirrups reached 600 με, through a round steel rod and a triangular steel wedge along the top and bottom v-slots of specimen, respectively.

After pre-cracked, the specimen was turned by 90° and placed vertically in the same test rig, as shown in Fig. 3b. The specimen was supported on roller bearings so that it could move freely in the horizontal direction to impose pure shear loading on the cracked plane.

3.5. Instrumentation

A loading cell was installed vertically on the end of the hydraulic jack to record the applied load. Two displacement transducers were placed vertically near the specimen centre on one side (Fig. 4a), and three horizontally on the other side (Fig. 4b), to measure the shear displacement and the crack opening widths, respectively. Electrical resistance strain gauges were pre-attached to stirrups to monitor the development of strain in the steel bars in order to quantify the lateral constraints, as shown in Fig. 5.

3.6. Loading scheme

Loading in the push-off tests was applied as follows. Before 60% of the estimated ultimate load P_u was reached, a loading increment $P_u/10$

Table 5
A summary of specimens and their details.

Specimen	Mix	RCA replacement rates (%)	Amount of stirrups	Cube strength (MPa)	Piece
N-12	1a	0	2Φ8	29.0	1
N-13			3Φ8		1
N-14			4Φ8		3
N-24	2	0	4Φ8	31.8	1
N-32	3	0	2Φ8	29.6	1
N-33			3Φ8		1
N-34			4Φ8		1
R-14	1c	100	4Φ8	19.3	2
R-42	4	100	2Φ8	27.0	1
R-43			3Φ8		1
R-44			4Φ8		3
R-52	5	100	2Φ8	33.8	1
R-53			3Φ8		1
R-54			4Φ8		1
R30-64	6	30	4Φ8	25.8	3
R50-14	1b	50	4Φ8	24.9	2
R50-72	7	50	2Φ8	24.7	1
R50-73			3Φ8		1
R50-74			4Φ8		3
R70-84	8	70	4Φ8	29.3	3

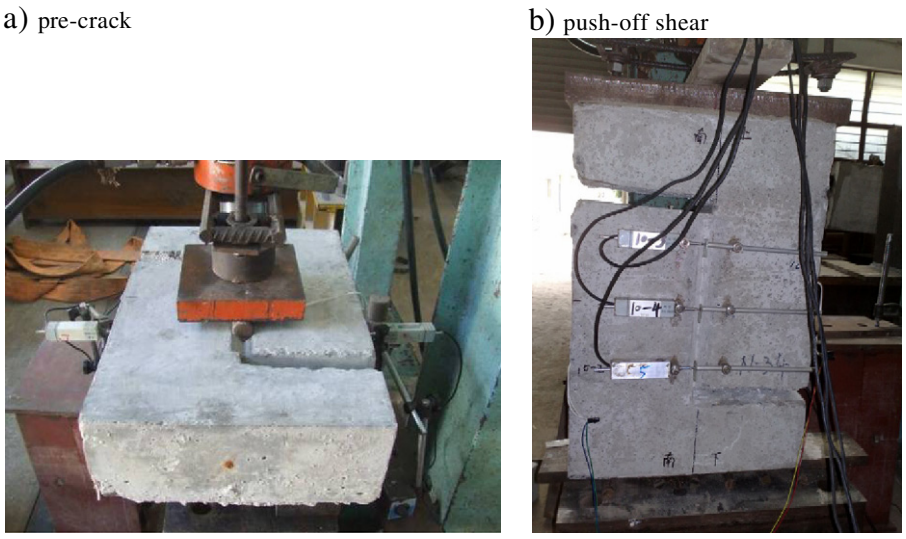

Fig. 3. The photos for test setup.

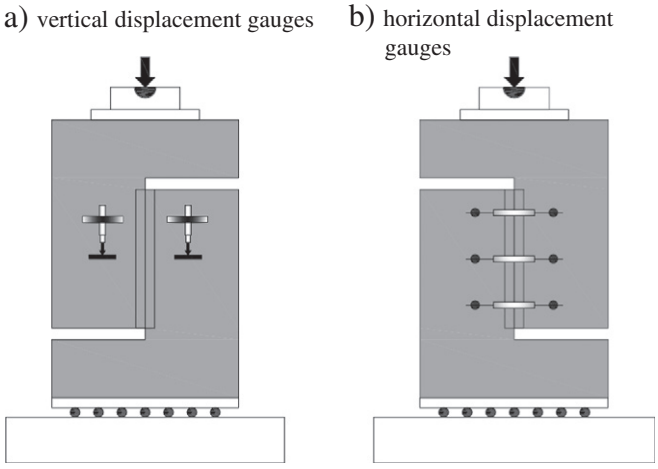

Fig. 4. Displacement transducer arrangement schematic.

was used. When the load was between 0.6–0.9P_u, the loading increment decreased to P_u/15. The test was held for 1–2 min after each loading step. After 0.9P_u was reached, the loading was controlled by vertical displacement at a loading rate 0.03 mm/min. The loading was stopped when the strain in the stirrups reached about 600 με, or equivalently when the crack width reached the serviceability limit 0.2 mm.

4. Experimental results

4.1. Failure modes

When the applied load was small, no cracks or crush could be seen on the specimen surfaces. When the load approached the ultimate load, some vertical shear cracks appeared on the specimen surfaces. The crack width increased with the increase of the shear displacement on both sides of the cracks. The specimens failed with much wider cracks width and shear displacement. The recordings from strain gauges showed that the stirrups had yielded.

There exists an only slight difference between all the failure and cracking patterns. Three representative crack patterns at failure are shown in Fig. 6a–c: one straight vertical crack, one kinked vertical crack, and a crack band with short diagonal cracks.

4.2. Main test results

Table 6 lists the main test results of all 32 specimens, including the uniaxial compressive strength of concrete f_c ($f_c = 0.76 f_{cu}$ [13]), the stirrup constraint stress on the shear plane $\rho_v f_{y,}$ where $\rho_v = A_v/A_c$ is the reinforcement ratio of the cross-sectional area of all stirrups A_v

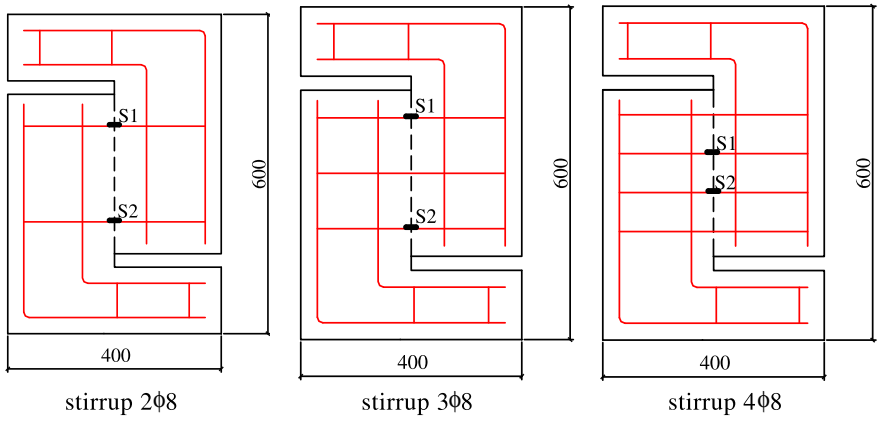

Fig. 5. Distribution of strain gauges.

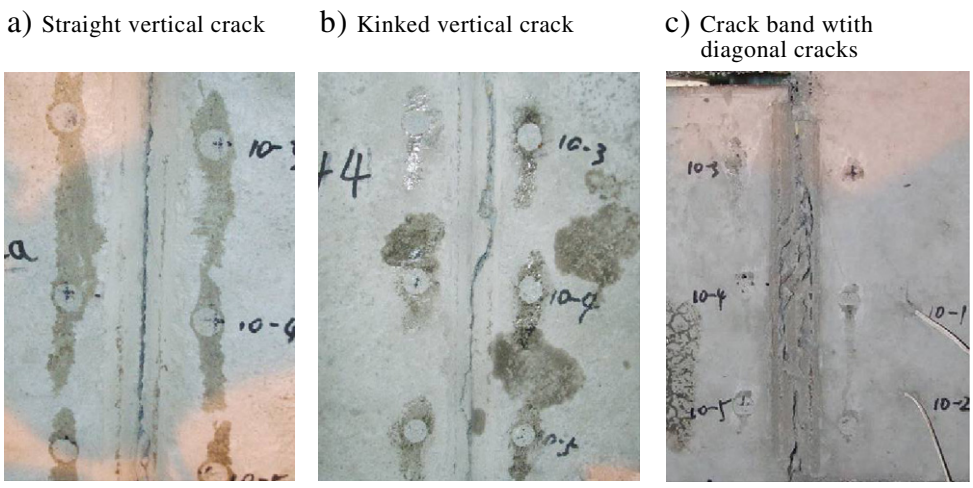

Fig. 6. Representative crack patterns of push-off specimens.

across the crack to the shear plane area A_c, and f_y is the yielding strength of stirrups; the ultimate shear load P_u; the ultimate shear stress $\tau_u = P_u/A_c$; the mean crack width measured in three positions w_u; and the shear displacement or slip Δ_u at the ultimate shear load.

From Table 6, it can be found that the ultimate shear stress τ_u increases with the increase of ρ_v, irrespective of RAC specimens or NAC specimens. The shear slip and the crack width at the ultimate shear stress are in the range of 0.46–1.26 mm and 0.24–1.16 mm, respectively.

Table 6
List of main test results.

Specimen	f_c(MPa)	$\rho_v f_y$(MPa)	P_u(kN)	τ_u(MPa)	w_u(mm)	Δ_u(mm)
N-12	22.0	1.9	–	–	–	–
N-13		2.9	184	5.10	0.44	0.65
N-14a		3.8	265	7.35	0.30	0.94
N-14b		3.8	273	7.59	0.29	0.98
N-14c		3.8	296	8.23	0.43	0.69
N-24	24.2	3.8	223	6.21	0.59	0.76
N-32	22.5	1.9	137	3.80	0.60	0.54
N-33		2.9	245	6.80	0.32	0.99
N-34		3.8	246	6.82	0.51	0.86
R-14a	14.6	3.8	230	6.39	0.54	0.73
R-14b		3.8	227	6.31	0.59	0.48
R-42	20.5	1.9	171	4.74	0.24	0.65
R-43		2.9	199	5.52	0.48	0.49
R-44a		3.8	264	7.34	0.46	0.54
R-44b		3.8	244	6.78	0.51	0.80
R-44c		3.8	222	6.18	0.31	0.73
R-52	25.7	1.9	154	4.27	0.46	0.81
R-53		2.9	220	6.12	0.21	0.47
R-54		3.8	245	6.80	0.50	0.46
R30-64a	19.6	3.8	286	7.93	1.16	1.26
R30-64b		3.8	295	8.20	1.01	0.79
R30-64c		3.8	290	8.05	0.56	0.89
R50-14a	18.9	3.8	242	6.72	0.64	0.84
R50-14b		3.8	238	6.60	0.45	0.91
R50-72	18.8	1.9	102	2.82	0.94	1.10
R50-73		2.9	220	6.10	0.85	0.76
R50-74a		3.8	249	6.93	0.52	0.80
R50-74b		3.8	251	6.97	0.38	0.82
R50-74c		3.8	232	6.45	0.80	0.79
R70-84a	22.2	3.8	244	6.78	0.46	0.66
R70-84b		3.8	238	6.62	0.74	1.07
R70-84c		3.8	253	7.02	0.68	0.97

N-12 has an operation mistake during testing.

4.3. Shear stress-shear displacement curves

The typical shear stress-shear displacement curves of a few specimens are plotted in Fig. 7. It can be seen that all the curves are of similar shape: a straight line representing linear elastic material behaviour in the early stage of loading and a nonlinear section representing the initiation and propagation of microcracks, followed by a short plateau near the peak load representing the stable propagation of macrocracks and finally along, nearly straight, decreasing line representing the forming of the major shear crack and the gradual loss of the aggregate interlock capability.

4.4. Shear slip-crack separation curves

Fig. 8a–f show typical shear slip-crack separation curves for six specimens. As the crack separations were measured at three vertical positions by horizontal displacement transducers, three curves are drawn in each of Fig. 8a–f. It can be found that in the initial period of loading, the crack width hardly changes. Before the ultimate shear load is reached, the crack has nearly the same width along the specimen depth.

It can also be noted from Fig. 8 that, the crack separation/opening curves for the RAC specimens with different R_r and for the NAC specimens share the same features. They are convex before the ultimate shear stress is reached. After that an inflection point appears, followed by quick growth of both crack width and shear slip and final failure.

5. Analysis of test results

5.1. Effects of the lateral constraint stiffness

Fig. 9a compares the shear stress-shear slip curves for the 5 RAC specimens of mix 4 (R-42, R-43, R-44a, R-44b and R-44c) with the same $R_r = 100\%$ but different stirrups. The curves for the 3 RAC specimens of mix 5 (R-52, R-53 and R-54), and the 5 specimens of mix 7 (R50-72, R50-73, R50-74a, R50-74b and R50-74c), are compared in Fig. 9b and c, respectively.

It can be seen that, compared with 2Φ8 lateral stirrups, the greater lateral constraint from more stirrups (3Φ8 or 4Φ8) leads to higher initial shear stiffness, higher shear stress for the same shear slip, and higher ultimate shear stress. From Fig. 9 and Table 6, the ultimate shear stress increased by 40–140% when the lateral stirrups increased from 2Φ8 to 4Φ8.

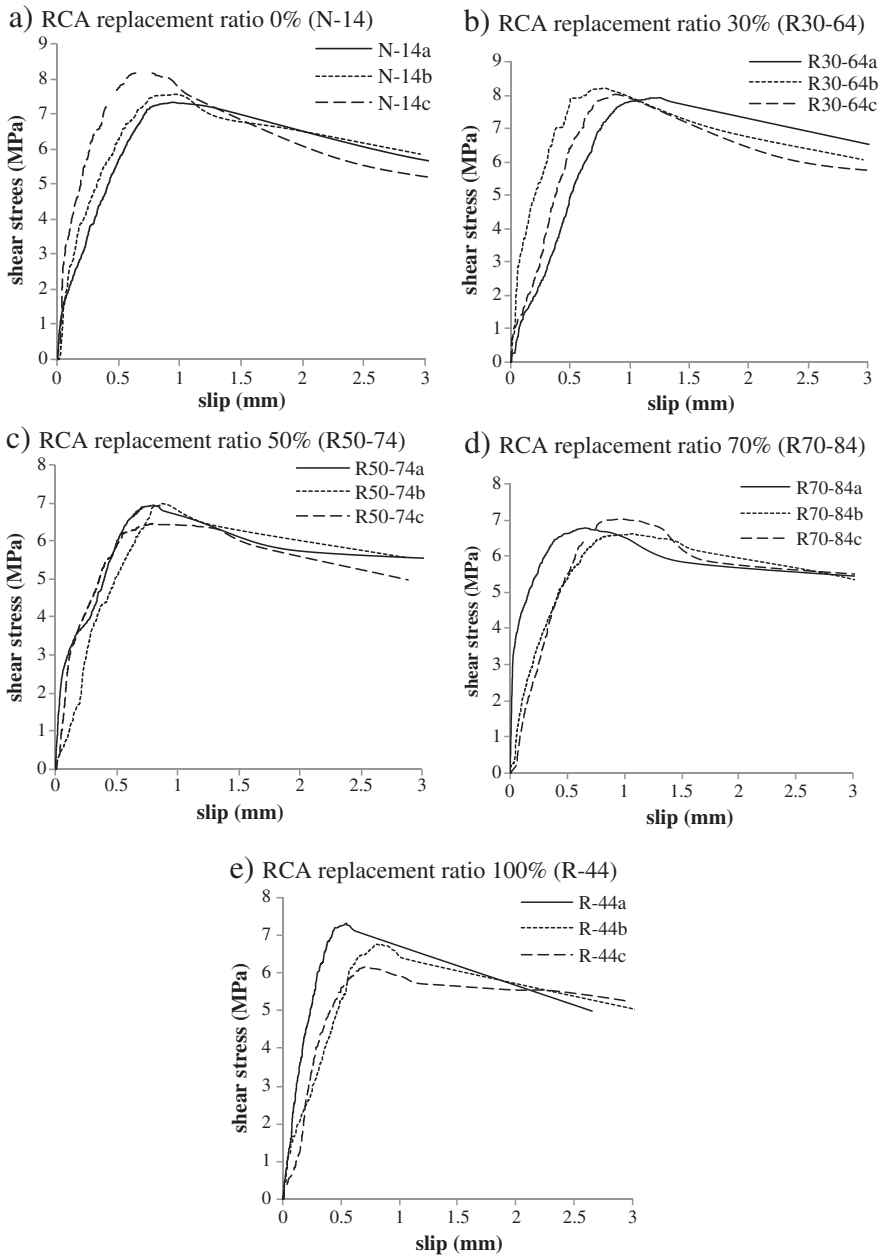

Fig. 7. Typical shear stress-shear displacement curves.

5.2. Effects of concrete strength

Fig. 10 compares the averaged shear stress–shear slip curves of three groups of specimens with the same R_r (=100%) and stirrups (4Φ8) and different compressive strength, namely R-14a and R-14b with f_c=14.6MPa, R-44a, R-44b and R-44c with f_c=20.5MPa, and R-54 with f_c=25.7MPa, as an example. It can be seen the initial shear transfer stiffness increases as f_c rises. Table 7 lists the average ultimate shear load $\overline{P_u}$ for the three groups of specimens. It can be seen that the ultimate shear stress of the RAC specimens tends to improve with the increase of concrete strength.

5.3. Effects of RCA replacement ratio with different water to cement ratio

Fig. 11 shows the variation of the ultimate shear loads P_u with R_r of five groups of specimens (3 specimens in each group) with different water to cement ratio but similar concrete strength ($f_c \approx 20$ MPa) and the same constraint stiffness (4Φ8 stirrups) but different R_r, namely, N-14 with R_r=0%, R30-64 with R_r=30%, R50-74 with R_r=50%, R70-84 with R_r=70%, and R-44 with R_r=100%. A broken line connecting the mean point of each group is also shown. It can be seen that the ultimate shear load of RAC is nearly the same as that of NAC for R_r<30%, but it reduces by nearly 15% from R_r=30% to 50%, after which it stabilizes with a value of $0.85P_u$ of NAC. It could be concluded that the RCA replacement ratio is one of the important parameters influencing the ultimate shear load. This could be explained by the micro- and meso structure feature of recycled aggregate concrete. With the improvement of the RCA replacement ratio, the old mortar as well as the old interfacial transition zones increases in the recycled aggregate concrete. These contribute to the reduction of the aggregate interlocking [14]. The detailed mechanism need further study in the future.

Fig. 12 displays the shear stress–shear displacement curve of N-14a, R50-74b, R-44b, respectively. From the ascending part of

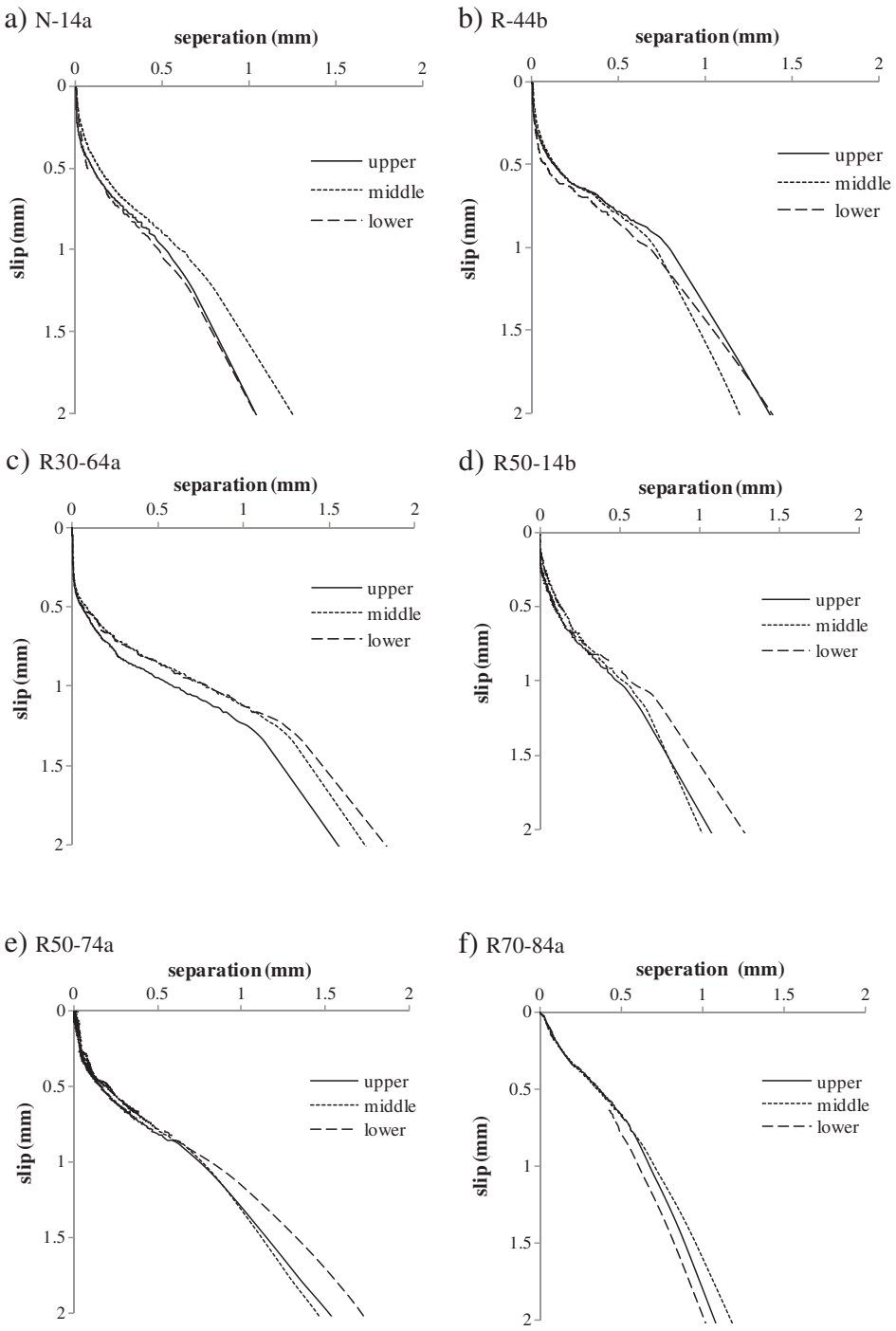

Fig. 8. Typical crack opening curve.

Fig. 12, it can be found that the basic performance of shear stress verse the slip is almost the same when the specimen has similar compressive strength and same restrains, irrespective of different RCA replacement percentage, i.e., 0%, 50% and 100%.

5.4. Effects of RCA replacement ratio with same water to cement ratio

Fig. 13 compares the shear stress–slip curves of three specimens, N-14a, R50-14a and R-14a, which have the same water to cement ratio (0.488), the same constrain stiffness (4Φ8), but different R_r (0, 50%, 100%). It can be seen that, R_r has little influence on the initial shear stiffness, however, a higher RCA replacement ratio R_r leads to a lower ultimate shear stress. This is because higher R_r leads to lower f_c of RAC with same water-cement ratio (f_c = 22.0MPa, 18.9MPa and 14.6MPa for N-14a, R50-14a and R-14a, respectively, from Table 6), and in turn, the lower f_c leads to a lower ultimate shear load, as already shown in Table 7. More experimental evidences of the adverse effects of R_r on f_c of RAC can be found in Refs. [15] and [16].

6. Prediction of the shear transfer strength

6.1. Comparisons of the test values and code values

A few design codes provide formulas to predict the shear transfer strength τ_u across cracks considering different constraint stiffness. For

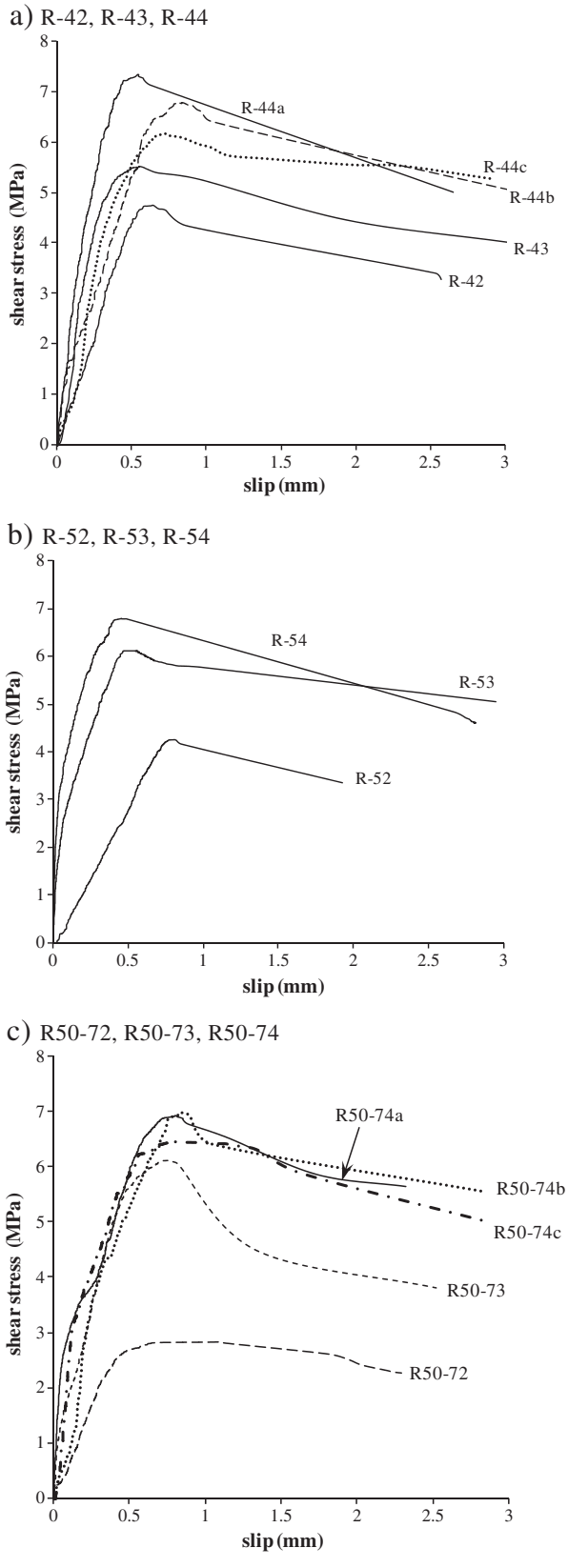

Fig. 9. Effects of constraint stiffness to shear stress-shear displacement curve.

example, ACI [17] and PCI [18] use Eqs. (1) and (2) to calculate τ_u, respectively

$$\tau_u = 1.4\frac{\rho_v f_y}{f_c'} \le 0.2 f_c' \le 5.5 \quad (1)$$

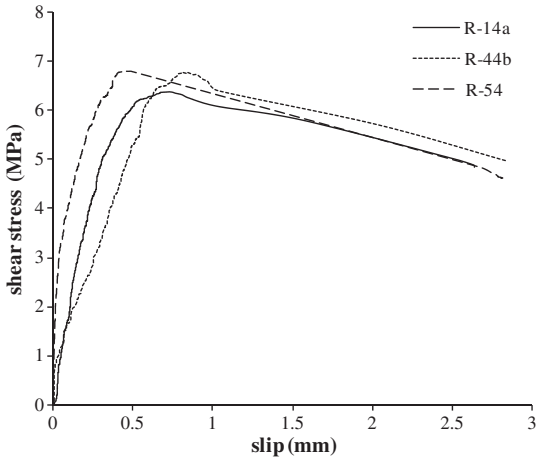

Fig. 10. Effects of concrete strength to shear stress-shear displacement curve.

$$\begin{cases} \tau_u = 1.4\dfrac{\rho_v f_y}{f_c'} & \dfrac{\rho_v f_y}{f_c'} < 4.14 \\ \tau_u = 1.4\left(\dfrac{2.07}{\rho_v f_y} + 0.5\right)\dfrac{\rho_v f_y}{f_c'} & \dfrac{\rho_v f_y}{f_c'} \ge 4.14 \end{cases} \quad (2)$$

where $\rho_v f_y / f_c'$ is the reinforcement index and $f_c' = 0.79 f_{cu}$ is cylinder compressive strength of concrete [19]. The other symbols have the same meanings as described in Section 4.2.

The predicted τ_u from Eqs. (1) and (2) for the 32 push-off specimens are compared with the test values in Table 8. The ratios of test values to predicted ones are also shown. It can be seen that, except for R-14a and R50-72, both equations underestimate the shear strength considerably, by 45–100% for Eq. (1) and 20–55% for Eq. (2), respectively. This indicates that both the ACI and PCI codes may be used to calculate the shear transfer strength of RAC with safety. The ACI code is much more conservative than the PCI code because a strict upper limit is specified by the former.

6.2. Comparisons between the test values and empirical formula

Besides design equations recommended by codes, different forms of empirical formula based on curve-fitting of experimental data also exist for the ultimate shear transfer strength prediction, such as linear in Eq. (3) by Mattock [20], bilinear in Eq. (4) by Mansur et al. [21] and nonlinear in Eq. (5) by Loov and Patnaik [22], all with a cap $\tau_u = 0.3 f_c'$

$$\frac{\tau_u}{f_c'} = \begin{cases} 2.25\left(\dfrac{\rho_v f_y}{f_c'}\right) & \dfrac{\rho_v f_y}{f_c'} < 0.069 \\ 0.1 + 0.8\left(\dfrac{\rho_v f_y}{f_c'}\right) & 0.069 \le \dfrac{\rho_v f_y}{f_c'} \le 0.25 \text{ for } f_c' \le 55 MPa \\ 0.3 & \dfrac{\rho_v f_y}{f_c'} > 0.25 \end{cases} \quad (3)$$

Table 7
Effect of compressive strength to the ultimate shear load.

Specimen	R-14	R-44	R-54
f_c (MPa)	14.6	20.5	25.7
P_u (kN)	229	244	245

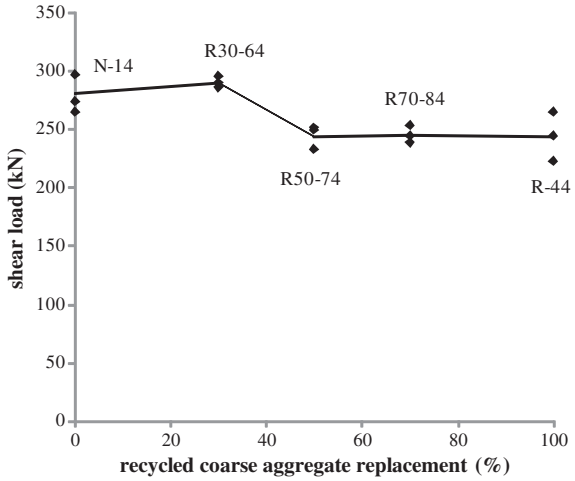

Fig. 11. Effect of RCA replacement ratio to shear load.

$$\frac{\tau_u}{f_c'} = \begin{cases} 2.5\left(\dfrac{\rho_v f_y}{f_c'}\right) & \dfrac{\rho_v f_y}{f_c'} < 0.075 \\ \dfrac{0.56}{(f_c')^{0.385}} + 0.55\left(\dfrac{\rho_v f_y}{f_c'}\right) & 0.075 \le \dfrac{\rho_v f_y}{f_c'} \le 0.27 \\ 0.3 & \dfrac{\rho_v f_y}{f_c'} > 0.27 \end{cases} \quad (4)$$

$$\frac{\tau_u}{f_c'} = 0.573\left(\frac{\rho_v f_y}{f_c'}\right)^{0.45} \le 0.3 \quad (5)$$

The test results of RAC specimens with $R_r = 100\%$, 50% and 0% are compared with the above equations using $f_c' = 20$ MPa in Fig. 14. It can be seen that the test results are mostly scattered above three empirical curves, indicating Eqs. ((3)–(5)) can also be used to predict the shear transfer strength at cracks of RAC.

7. Conclusions

Based on the experimental studies and data analysis of 32 push-off specimens, the following conclusions can be drawn:

(1) Overall, in terms of the shape of shear stress-slip curves and the crack propagation paths, the shear transfer performance across cracks in RAC is similar to that in NAC.

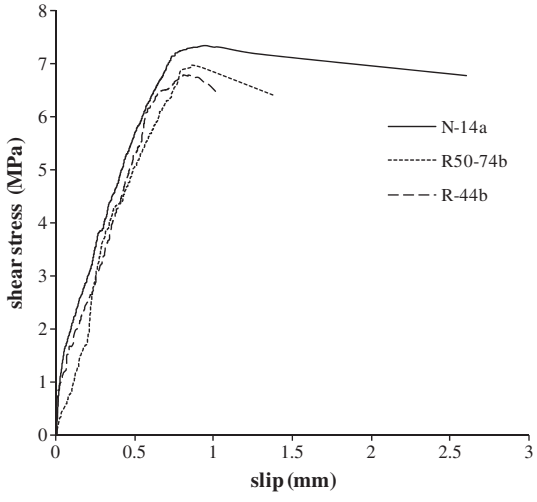

Fig. 12. Effect of RCA replacement ratio to shear stress–slip curve.

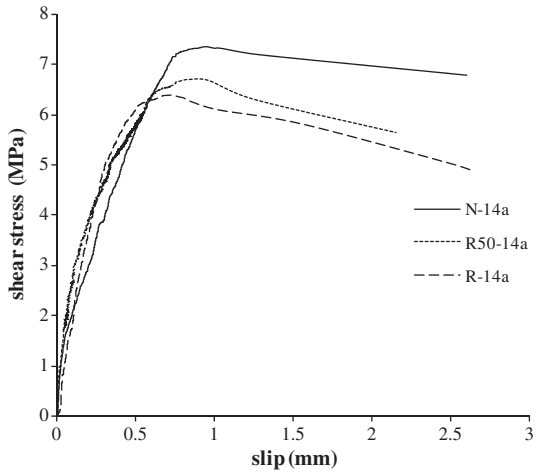

Fig. 13. Shear stress–slip curve with same mix proportions.

(2) For RAC specimens with same mix designs, the shear transfer performance, including the initial stiffness and ultimate shear strength, is significantly improved with the increase of lateral constraint stiffness.
(3) The RCA replacement ratio R_r has significant effects on the ultimate shear load P_u of specimens with similar concrete strength (different water to cement ratios) and same constrain stiffness. P_u of RAC is nearly the same as that of NAC for $R_r < 30\%$, but it reduces from $R_r = 30\%$ to 50%, after which it stabilizes at about $0.85P_u$ of NAC. Its influence on the initial shear stiffness is negligible.
(4) Lower R_r leads to higher concrete strength, which in turn results in higher ultimate shear load for RAC specimens with the same water-cement ratio (different compressive strength) and lateral constraint stiffness.

Table 8
The shear strength τ_u from the test and codes.

Specimen	Test(MPa)	ACI (MPa)	Test:ACI	PCI (MPa)	Test:PCI
N-13	5.10	3.99	1.28	3.99	1.28
N-14a	7.35	4.57	1.61	5.32	1.38
N-14b	7.59	4.57	1.66	5.32	1.43
N-14c	8.23	4.57	1.80	5.32	1.55
N-24	6.21	5.02	1.24	5.32	1.17
N-32	3.80	2.66	1.43	2.66	1.43
N-33	6.80	3.99	1.70	3.99	1.70
N-34	6.82	4.67	1.46	5.32	1.28
R-14a	6.39	3.04	2.10	5.32	1.20
R-14b	6.31	3.04	2.07	5.32	1.19
R-42	4.74	2.66	1.78	2.66	1.78
R-43	5.52	3.99	1.38	3.99	1.38
R-44a	7.34	4.26	1.72	5.32	1.38
R-44b	6.78	4.26	1.59	5.32	1.27
R-44c	6.18	4.26	1.45	5.32	1.16
R-52	4.27	2.66	1.61	2.66	1.61
R-53	6.12	3.99	1.53	3.99	1.53
R-54	6.80	5.32	1.28	5.32	1.28
R30-64a	7.93	4.07	1.95	5.32	1.49
R30-64b	8.20	4.07	2.01	5.32	1.54
R30-64c	8.05	4.07	1.98	5.32	1.51
R50-14a	6.72	3.93	1.71	5.32	1.26
R50-14b	6.60	3.93	1.68	5.32	1.24
R50-72	2.82	2.66	1.06	2.66	1.06
R50-73	6.10	3.9	1.56	3.99	1.53
R50-74a	6.45	3.9	1.66	5.32	1.21
R50-74b	6.97	3.9	1.79	5.32	1.31
R50-74c	6.93	3.9	1.78	5.32	1.30
R70-84a	6.78	4.62	1.47	5.32	1.27
R70-84b	6.62	4.62	1.43	5.32	1.24
R70-84c	7.02	4.62	1.52	5.32	1.32

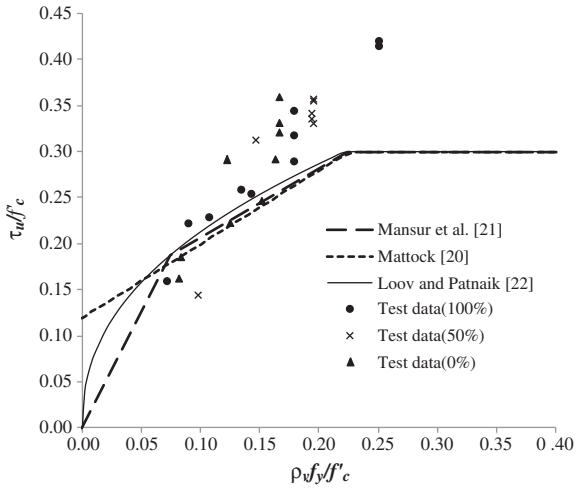

Fig. 14. Comparisons between tested value and empirical formula.

(5) Both the Eqs. ((1) and (2)) recommended by ACI and PCI and Eqs. ((3)–(5)) for NAC can be used to predict the shear transfer strength across cracks in RAC. However, further tests, analytical and micro/meso-scale numerical studies are needed to develop more accurate equations specific to RAC.

Acknowledgments

The work was financially supported by the National Science Foundation (50738005) and the Shanghai Science and Technique Committee (No. 10231202000). J. Xiao also highly appreciates the support of the German Research Foundation (DFG, Project-No. ZH15/18-1). Special thanks are given to Prof. Dr. -Ing. Ch. Zhang in Siegen University and Miss Chang Sun in Tongji University.

Appendix A. Supplementary data

Supplementary data to this article can be found online at doi:10.1016/j.cemconres.2012.02.006.

References

[1] R. Parker, T. Paulay, Reinforced Concrete Structures, John Wiley & Sons, New York, 1975.
[2] T. Paulay, P.J. Loeber, Shear transfer by aggregate interlock, ACI special publication, , 1974, pp. 1–15.
[3] J.C. Walraven, H.W. Reinhardt, Theory and experiments on mechanical behaviour of cracks in plain and reinforced concrete subjected to shear loading, Heron 26 (1981) 5–68.
[4] J.C. Walraven, Aggregate interlock: A theoretical and experimental investigation, Thesis presented to the Delft University of Technology, at Delft, The Netherlands. 1980, in partial fulfillment of the requirements for the degree of Doctor of Philosophy.
[5] R.C. Fenwick, T. Paulay, Mechanisms of shear resistance in concrete beams, J. Struct. Div., ASCE 94 (1968) 2235–2350.
[6] H.P.J. Taylor, Investigation of the dowel shear forces carried by the tensile steel in reinforced concrete beams, Cement and Concrete Association, Technical Report 42.431, 1969 London.
[7] H.P.J. Taylor, Investigation of the forces carried across cracks in reinforced concrete beams in shear by interlock of aggregate, Cement and Concrete Association, Technical report 42.447, 1970 London.
[8] J.P. Laible, R.N. White, P. Gergely, Experimental investigation of seismic shear transfer across cracks in concrete nuclear containment vessels, ACI Special Publication SP-53, 1977, pp. 203–226.
[9] R. Jimenez, P. Gergely, R.N. White, Shear Transfer Across Cracks in Reinforced Concrete, Report 78-4, Cornell University, Ithaca (N.Y.), 1978, p. 357.
[10] M.N. Fardis, O. Buyukozturk, Shear transfer model for reinforced concrete, J. Struct. Div., ASCE 105 (1979) 255–275.
[11] Z.J. Yang, X.T. Su, J.F. Chen, G.H. Liu, Monte Carlo simulation of complex cohesive fracture in random heterogeneous quasi-brittle materials, Int. J. Solids Struct. 46 (2009) 3222–3234.
[12] M. Haskett, D.J. Oehlers, M.S. Mohamed Ali, S.K. Sharma, The shear friction aggregate interlock resistance across sliding planes in concrete, Mag. Concrete Res. 62 (2010) 907–924.
[13] J.Z. Xiao, J. Li, Ch. Zhang, Mechanical properties of recycled aggregate concrete under uniaxial loading, Cement Concrete Res. 35 (2005) 1187–1194.
[14] J.Z. Xiao, W.G. Li, Zh. Sun, Crack propagation in recycled aggregate concrete under uniaxial compressive loading, ACI Materials Journal 109 (2012).
[15] J.Z. Xiao, W.G. Li, Y.H. Fan, X. Huang, A review of study on recycled aggregate concrete in China (1996–2011), Construction and Building Materials 31 (2012) 364–383.
[16] M. Etxeberria, E. Vázquez, A. Marí, M. Barra, Influence of amount of recycled coarse aggregates and production process on properties of recycled aggregate concrete, Cement and Concrete Research 37 (2007) 735–742.
[17] American Concrete Institute (ACI), Building code requirements for structural concrete, No. 318-2005, Committee 318, Farmington, Hills, Mich, 2005.
[18] Prestressed Concrete Institute (PCI), PCI design handbook, 4th ed. PCI, Chicago, 1992.
[19] Gu. Xianglin, The Basic Principle of Concrete Structures, Tongji University Press, Shanghai, 2011 (in Chinese).
[20] A.H. Mattock, Shear friction and high-strength concrete, ACI J. 69 (2001) 50–59.
[21] M.A. Mansur, T. Vinayagam, Kiang-Hwee Tan, Shear transfer across a crack in reinforced high-strength concrete, J. Mater. Civil Eng., ASCE 20 (2008) 294–302.
[22] R. Loov, A. Patnaik, Horizontal shear strength of composite concrete beams with rough interface, PCI J. 39 (1994) 48–67.